MODELLING OF INITIAL DEPOSITION OF BIOMASS ASH PARTICLES ON WALLS OF SUPERHEATER TUBES

by

Yibin WANG, Hexin LIU, and Houzhang TAN*

MOE Key Laboratory of Thermo-Fluid Science and Engineering,
School of Energy and Power Engineering, Xi'an Jiaotong University, Xi'an, Shaanxi, China

Original scientific paper
https://doi.org/10.2298/TSCI200311270W

Condensation of gaseous alkali chloride and sulphate and adhesion of molten ash particles are still an important issue of investigation and gaining more and more attention in biomass utilization. In this work the behaviours for formation of initial deposition layer and condensation of KCl(g) and $K_2SO_4(g)$ *were simulated numerically in a 2-D computational domain of an in-line 4×4 tube bundle. The sticking and rebound efficiency of incident particles, condensation rate of gaseous salts and ash deposition rate on both of the windward and the leeward sides of tubes were obtained through transient calculation cases. The ash deposition mass on the windward side of tubes is mainly from impaction and stickiness of large ash particles. The condensation rate of KCl(g) is two orders of magnitude higher than that of* $K_2SO_4(g)$ *on both of the windward and the leeward side of tubes. The ash deposition rate and the condensation rate on the windward side of tubes are of equal importance. While on the leeward side of tubes the condensation of salt vapours is more dominant than the inertial impaction in the forming stage of initial layer.*

Keywords: *condensation, biomass, ash particles, stickiness, modelling*

Introduction

Biomass as a CO_2 zero emission fuel has important potentials in these aspects of environmental pollution reduction, fossil fuel replacement, heat and electricity supply. The proportion of power generation from biomass combustion or biomass gasification coupled with its by-products combustion is gradually increased in many countries such as Denmark, Finland, and the United Kingdom [1]. After completing the mission of ultra-low emission retrofits for most of coal-fired power plants in China, the Chinese government is trying their best efforts to develop the biomass utilization technologies to meet heat and power supply for villages and small cities or towns. However, straw or woody biomasses usually contain large amounts of alkali metal chlorides and sulphates, and they have a low softening temperature ranged from 650 °C to about 1000 °C [2, 3]. This property easily induces ash deposition, slagging and corrosion on heating surfaces and then affects the stable operation of boilers. Ash deposition on walls involves many sub-processes such as fluid-flow, heat and mass

---

[*] Corresponding author, e-mail: hzt@mail.xjtu.edu.cn

transfer, gas-to-solid conversion of alkali salt vapours [4, 5], so to make more precise evaluations on this behaviour is still a challenge.

The CFD as a powerful tool is often used for solving complex multi-phase flow, chemical reactions and solid fuel combustion in boilers. But some assumptions and simplifications in length and time scales need to be made for better solving the problems and further reducing the computation time and cost. Ash-related issues often cause some unscheduled shutdowns of boilers. So, developing an appropriate model to well simulate or predict ash deposition rate and deposit shapes at different stage is of great importance. Weber *et al.* [6] reviewed some sticking models for predicting ash deposition by CFD and recognized that some composition-dependent deposition models with considering more factors need to be improved in future investigation. Mu *et al.* [7] found the large particles had a high deposition trend onto the windward side of tubes, and high temperature would improve ash deposition on walls in a wastewater incinerator. Perez *et al.* [8] developed a new deposition model that is suitable for predicting the shapes of ash deposition in a tube bank of a Kraft recovery boiler. Generally, in comparison with the movement of ash particles, the condensable species arrive firstly onto the cool surface of a clean heat transfer tube. During low grade solid fuels combustion large amounts of condensable species will be produced, which suggests a significant influence on the deposit built-up. But in these aforementioned studies, the condensation of salt vapours is not happened due to medium flue gas temperature. While for low grade solid fuels such as biomass and lignite, release, transformation and vapour condensation of inorganic salts at high temperature (>1000 °C) are common. Wang and Tan [9] and Wang *et al.* [10] used an evaporation-condensation experimental device to study the condensation behaviour of the vapours released from straw biomass, condensation rate of pure KCl(g) and its gas-to-solid conversion. Akbar *et al.* [11] investigated the condensation of K_2SO_4 on a single probe using code AIOLOS, and they suggested that the film theory was able to more reasonably predict the condensation behaviour on the deposition probe. Forstner *et al.* [12] studied the condensation of ash-forming elements and ash deposition in a subsequent fire tube boiler. They found the condensation behaviour tends to appear on walls of the fire tube with a low temperature. Salt vapour condensation behaviour is temperature dependent. It plays an important role in ash deposit growth, but this process involving many mechanisms is not clear. Therefore, more thorough experiments and modelling will be greatly encouraged for figuring out each sub-process and revelling the conversion of gaseous condensable species.

Although many experimental and numerical studies have been done for further understanding the process of ash deposition, more attention is still paid to the deposition characteristics of ash particles at a steady-state. It is well-known that the deposit growth rate and depositing composition change with flow time. The changing boundary condition will affect the behaviour of condensable species. Many collected deposits show similar enrichment characteristic of potassium or sodium chlorides and sulphates. For high alkali solid fuels, neglecting the contribution of inorganic vapour condensation may underestimate the overall ash deposition rate around a tube. The numerical simulation could provide more information on condensation behaviour in comparison with experimental investigation. There is still less investigation conducted to quantitatively evaluate the importance of vapour condensation in the overall deposition rate during the formation stage of initial deposition. Therefore, this work aims to give more details and basic knowledge on this behaviour through CFD transient simulation, such as particle impaction, rebound, stickiness and direct condensation of salt vapours on the surfaces of superheater tubes, in order to better understand the formation and development behaviour of initial deposit layer.

Model description

In the following content, the computational domain of an in-line 4×4 tube bundle and its boundary conditions will first be presented. The equations for continuum and discrete phases will be illustrated in the next section. Finally, the models for vapour condensation and ash deposition will be discussed in detail.

Computational domain

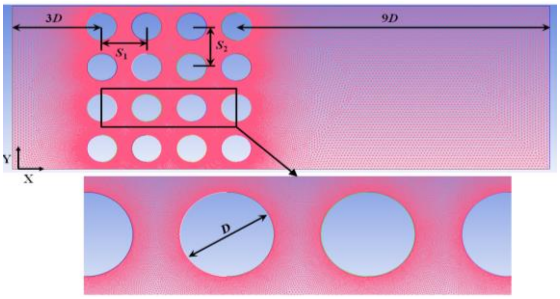

Figure 1. Schematic diagram of computational domain of 4×4 tube bundle

As presented in fig. 1, an in-line 4×4 tube bundle geometry is chosen as the computational domain, which is representative for super-heaters located at the exit of furnace in a 12 MW biomass-fired power plant. This tube bundle geometry was simulated to be operating with an upstream flue gas velocity of 6 m/s, a tube surface temperature of 764 K, and a flue gas temperature of 1274 K at inlet. More details on this biomass furnace can be found in [13]. The diameter, *D*, of a tube in this tube bundle is 38 mm and its longitudinal pitch S_1 remains 2*D* between the centres of the tubes, tab. 1. The inlet width of computational domain is set to 228 mm. The distance from the inlet to the centre of tubes at first row is set to 3*D* and the length from the centre of tubes at the forth row to the exit remains 9*D*. Here four types of boundary conditions were used for the computational domain. The flue gases at the inlet were assumed to be mainly consisted of 15.3% CO_2, 3.2% O_2, 11% H_2O, and 70% N_2. Meanwhile minor of $KCl_{(g)}$ and $K_2SO_{4(g)}$ was contained in flue gases, which were approximate to $3.5\cdot10^{-4}$ and $1.6\cdot10^{-6}$, respectively, as calculated using CHEMKIN by Garba *et al.* [4]. At the inlet boundary, the flue gases were assumed to have a uniform velocity and temperature, and its turbulent intensity of 5.22% which can be obtained by the formula of 0.16 $Re^{-0.125}$. No-slip conditions and constant temperature were employed for the surface of tubes. The boundary conditions for top and bottom of this domain were set to be periodic and symmetry, respectively. A pressure condition was set at the exit of computational domain.

Table 1. Elemental distributions of the three fouling deposit samples

Parameters	Value
Tube diameter [mm]	38
Longitual pitch [mm]	76
Transverse pitch [mm]	76
Flue gas velocity [ms^{-1}]	6
Flue gas temperature [K]	1274
Surface temperature of a tube [K]	764
Tube material	Steel
Heat conduction coefficient [$Wm^{-1}K^{-1}$]	27.96
Parameters	Value

The pre-processor GAMBIT was used for the whole computational domain to generate the unstructured meshes. Verification of grid independence was performed by varying the node number around a tube from 24 to 840, and finally the node number of 360 was chosen because of no influence on impacting efficiency on the windward side of a tube. The node number was the same as suggested by Weber *et al*. [6]. Finally, about 296000 meshes for the whole domain were adopted.

Continuum and discrete phase modelling

The conservation equations in Cartesian co-ordinates for mass, species, momentum and energy have a similar structure and can be found in elsewhere [14], so which will not be presented here. For the flow conditions in the present work, the standard k-ε, the RNG k- ε and the k-ω SST (shear-stress transport) can be considered for simulating eddy viscosity. But the k-ω SST combines the benefits of both the k-ω model and the k-ε model. In order to gain more accurate predictions in the boundary-layer region around tubes and well simulation of free stream flows, therefore, the k-ω SST was employed to consider the effect of turbulent flow.

The motion of ash particles was numerically described in a Lagrangian approach using the following equation, with considering the possible forces including the drag force, the thermophoretic force, the Saffman's lift force and the Brownian force:

$$\frac{\mathrm{d}u_p}{\mathrm{d}t} = \sum_i F_i \tag{1}$$

In calculation the ash particles were viewed to be non-spherical, and its drag coefficient was calculated using the correlation proposed by Haider and Levenspiel [15]. Here the shape factor for the correlation aforementioned was set to 0.7. The thermophoretic force acting upon a particle can be described by:

$$\vec{\mathrm{F}} = -\frac{6\pi \mathrm{d}_p \mu^2 C_\mathrm{s}\left(K + C_\mathrm{t}\mathrm{Kn}\right)}{\rho\left(1+3C_\mathrm{m}\mathrm{Kn}\right)\left(1+2K+2C_\mathrm{t}\mathrm{Kn}\right)}\frac{1}{m_p T}\nabla T \tag{2}$$

where the Knudsen number is defined as the ratio of the mean free path to the particle radius, K is defined as the ratio of fluid thermal conductivity to particle thermal conductivity, the coefficients C_s, C_t, and C_m were 1.17, 2.18, and 1.14, respectively. For other forces upon ash particles, the corresponding terms in the panel were enabling before the starting of calculation.

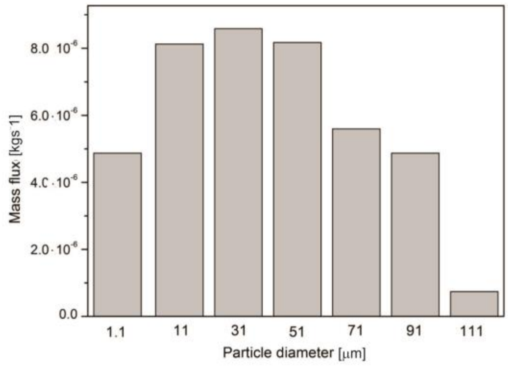

Figure 2. The mass flux of injecting ash particles with different diameter

The diameter of ash particles with a same density of 2600 kg/m^3 was ranged from 1.1 μm to 111 μm. The data on mass flux for injecting ash particles with different diameter was from [4], fig. 2. The injection procedure of ash particles was terminated over 11-time steps, and about 8778 particles were released into the computational domain. The dispersion of ash particles was described by using a stochastic tracking model with random eddy lifetime.

Condensation of alkali salt vapours

The direct condensation of gaseous alkali metal chlorides and sulphates onto the surfaces of deposits is also one of the most deposition mechanisms. In this case the nucleation, agglomeration and growth of salt vapours were not considered, only its direct condensation flux was calculated by:

$$m_{\mathrm{cond},i} = \beta_i M_i \left(\frac{P_i}{\mathrm{R}T_g} - \frac{P_{\mathrm{s},i}}{\mathrm{R}T_\mathrm{s}} \right) \tag{3}$$

where β_i is the mass transfer coefficient of $\mathrm{KCl}_{(g)}$ or $\mathrm{K_2SO_{4(g)}}$, m/s, and it can be obtained via an appropriate correlation for Sherwood number, P_i – the partial pressure of alkali salt vapours at bulk gas temperature T_g, $P_{\mathrm{s},i}$ – the saturation pressure of alkali salt vapours at the deposit surface temperature $T_\mathrm{s,}$ which is calculated using the formula proposed by Tomeczek *et al*. [16], M_i – the molar mass of $\mathrm{KCl}_{(g)}$ or $\mathrm{K_2SO_{4(g)}}$, and R – the universal gas constant. When the flue gas flowing into boundary-layer around the tube wall and its temperature started to decrease, the condensation of salt vapours occurs and releases some latent heat, the corresponding source terms are also added for continuity, species and energy equations via user-defined function.

Stickiness model for ash particles

The stickiness of an impacting particle is dependent on both the sticky properties of ash particle and the impacting wall. Here the sticking propensity of ash particles is described:

$$P_\mathrm{total} = P_\mathrm{ash} + \left(1 - P_\mathrm{ash}\right) P_\mathrm{wall} \tag{4}$$

At present several models have been developed for deciding the stickiness or rebound behaviour of ash particles after impaction, which including critical melting fraction, critical viscosity and excess energy, in order to better predict the formation of ash deposition by CFD simulations. Generally, straw and woody biomass ashes have a characteristic of alkali metal-rich and silicate-rich, and they have a low soften temperature of about 650-700 °C. The melting fraction as a crucial parameter for biomass ashes is often used for deciding particle sticking/rebound. Here, the stickiness propensity of ash particles was calculated via its melting fraction. In this work, straw biomass ash was assumed to be viewed as a mixture of alkali salt-rich component and silicate-rich component, whose melting fraction varying with temperature can be obtained by:

$$f_\mathrm{melt}\left(T, X_\mathrm{KCl}\right) = f_\mathrm{melt,KCl}\left(T\right) \frac{X_\mathrm{KCl}}{X_\mathrm{total}} + f_\mathrm{melt,silicates}\left(T\right) \frac{X_\mathrm{silicates}}{X_\mathrm{total}} \tag{5}$$

The melting function of KCl and silicates is greatly dependent on temperature, which can be viewed in [17]. For an impacting particle, its stickiness propensity can be decided by [12]:

$$P_\mathrm{ash} = \left\{ \begin{matrix} 0 & 0 < f \le 0.15 \\ 1.67 f - 0.167 & 0.15 < f \le 0.7 \\ 1 & f > 0.7 \end{matrix} \right\} \tag{6}$$

A lower melting fraction of 10% in some studies was chosen to be the critical value in the case of no deposition occurred on walls. The stickiness propensity remains linear increased when the fraction of biomass ash is higher than 15% but lower than 70%. Once the melting ash particles higher than 70%, its stickiness propensity will be 100%. When the ash particle impacting upon the surface, the code has to access the information on temperature and chemical composition of the impacting particles for calculating the stickiness propensity. If the sticking propensity of an impacting particle was not zero after a comprehensive evaluation, the tracking in next iteration will be aborted after writing the particle mass into corresponding variable.

Solution procedure

The 2-D and unsteady-state numerical simulation was carried out using fluent code combined with some user-defined functions to gain more data on variables. The periodic time in generation, growth and shedding of vortex behind the tubes at first row was approximate to 17 ms after carefully observing the calculating results. So in calculation a time step of 0.05 ms was chosen for better capturing the instantaneous characteristic of turbulent vortex in one vortex shedding period and its effect on the tracking of ash particles. A second-order discretization scheme was adopted for both convective and diffusive terms. All transport equations were solved using SIMPLE for providing the pressure correction for pressure and velocity coupling. The numerical calculation was recognized to be converged when the residual of each variable was less than 10^{-5}.

Results and discussion

Figure 3 gives the sticking and the rebound efficiency of incident particles. Here the sticking efficiency is defined as the ratio of the number of ash particles sticking on surfaces after impaction to that of ash particles impacting on surfaces. The rebound efficiency is defined as the ratio of the number of ash particles rebounding from surfaces after impaction to that of ash particles impacting on surfaces. On the windward side of tubes at the first row, the sticking efficiency is high up to 70%, but no ash particles adhere on the leeward side.

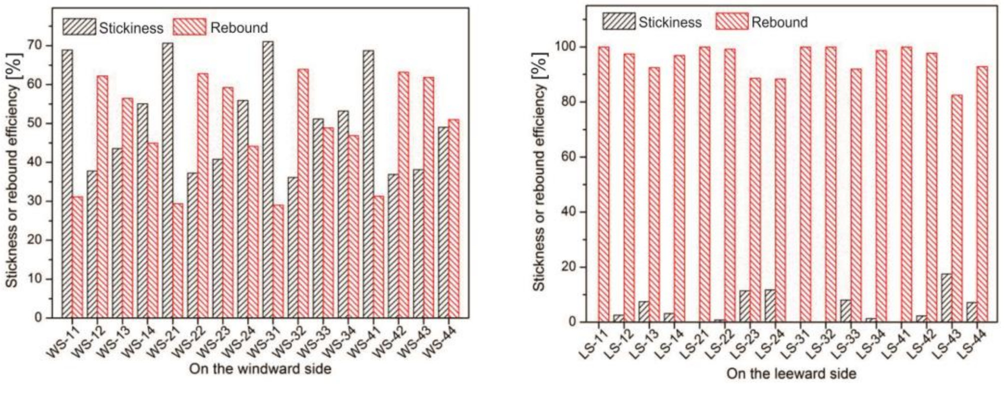

(a) **(b)**

Figure 3. Sticking and rebound efficiency of incident particles

For the second row, the sticking efficiency of impacting particles is decreased to around 38%. Accordingly, it has high rebound efficiency on the windward side of tubes, due to the swinging flow after flowing over the first row and more vortexes generated from boundary-layer separation. After flowing over the second row, the sticking efficiency of ash particles on the windward side of tube appears to be higher than 50%. Compared with the windward side, a high rebound efficiency of ash particles is appeared on the leeward side for most of tubes. This suggests that the entrained particles do not adhere on the leeward side under turbulent vortex and thermophoretic forces.

The stickiness or rebound of incident particles greatly depends on the sticking model. Here the sticking propensity for biomass ash deposition is accurate, because of the coupling consideration in the sticky capabilities of ash particles and impacting walls. The rebound criterion for an impacting particle is that the melt fractions of impacting particle and deposits layer are lower than 15%. Higher rebound efficiency appears on the leeward side of tubes rather than that on the windward side, due to lower particle temperature within backflow regions.

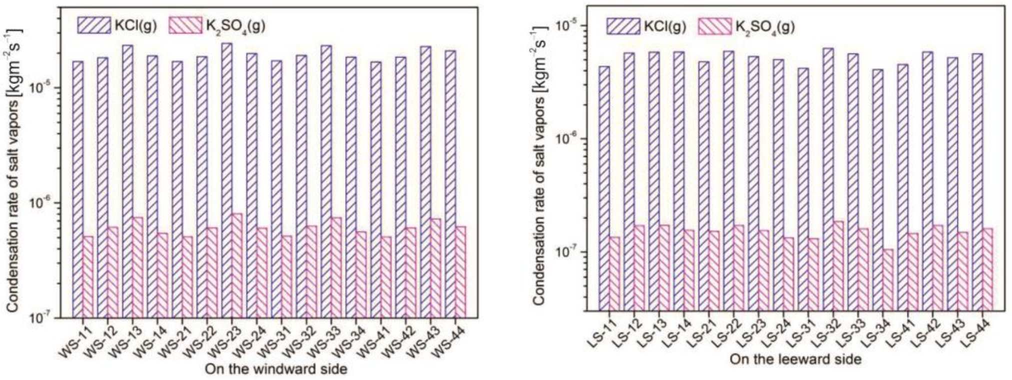

(a) **(b)**

Figure 4. Condensation rate of $KCl_{(g)}$ and $K_2SO_{4(g)}$

During flue gas temperature decreasing, some sub-processes will also be happened including nucleation, agglomeration and heterogeneous condensation of gaseous potassium chloride and sulphate into aerosols. Here the direct condensation of salt vapours onto the cooled surfaces is considered only in simulation. In comparison with gaseous potassium chloride, the gaseous potassium sulphate more easily tends to condense into nucleus because of a lower partial pressure when flue gas temperature decreases. Figure 4 presents the condensation rate of gaseous potassium chloride and sulphate. It can be found that, the condensation rate on the windward side is higher than that on the leeward side, due to a higher mass transfer coefficient in regions around the windward side. On both of the windward side and the leeward side of all tubes, the condensation rate of gaseous potassium chloride is observably higher than that of gaseous potassium sulphate, due to the difference in molar concentration. Actually, at the exit of a biomass firing boiler, the gaseous salt vapours not only condense onto the walls and the surfaces of ash particles but involving into the sulphation reaction with SO_2 or SO_3 and silication reaction with silica in ashes. Although the sulphation or silication reaction would reduce the concentration of gaseous potassium chloride and then decrease its condensation rate, large amounts of fine particles covered by condensed salts within the thermal boundary further promote the deposition rate. Moreover, the silication reaction would accelerate the formation of molten particles with a low melting temperature, further promote the formation of slagging on walls.

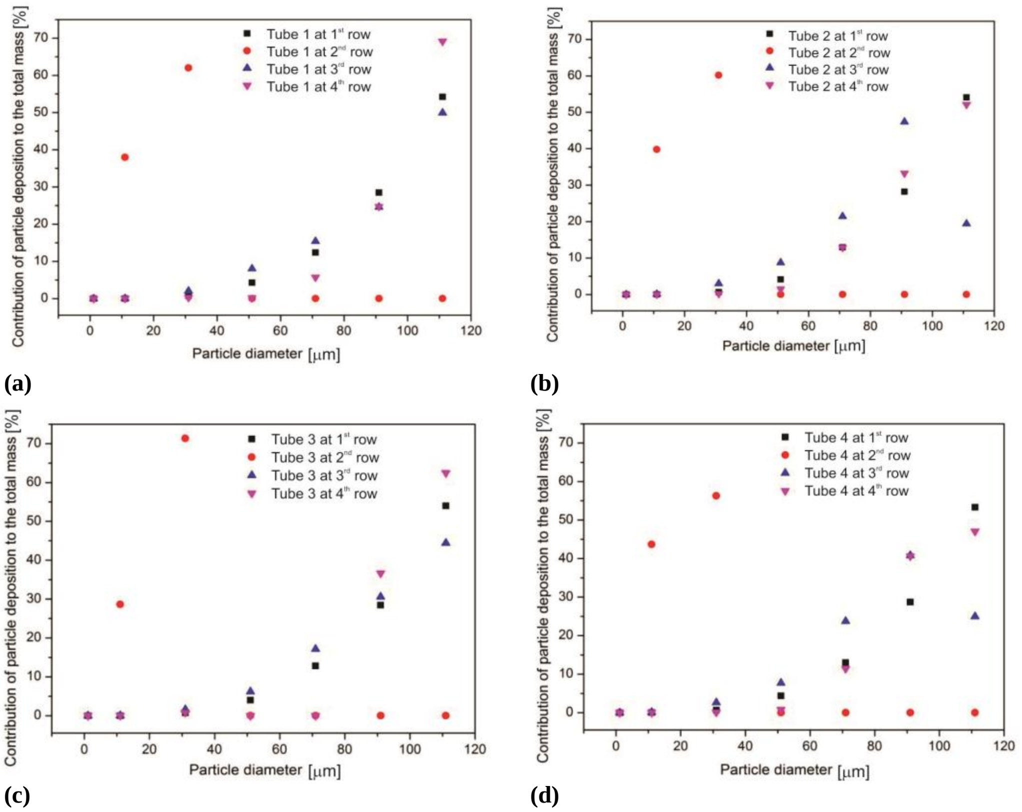

(a) (b) (c) (d)

Figure 5. Contribution of deposition of ash particles to total deposition mass on the windward side

Figure 5 shows the contribution of stickiness of ash particles with different diameter to the total deposition mass. For tubes at same row, there is a similar distribution characteristic of deposited particles with different size to the total deposit. For particles with a diameter of 1.1 μm, no deposition is found on the windward side of all tubes, due to a better following ability with the fluid. At the second row, the contributor to the deposit on the windward side is mainly from the stickiness of ash particles with diameters of 11 μm and 31 μm. While for tubes at other rows, the main contributor to the deposit is from the sum of ash particles larger than 31 μm. Moreover, the contribution percentage is increased with an increase in particle diameter. The contributor of large particles to the deposit is of significance and their behaviours affect its shape and irregularity [3, 18].

Figure 6 gives the contribution characteristic of particles with different diameter to the total deposit mass on the leeward side of all tubes. It can be found that, there is no deposition appeared on the leeward side of the first, the third and the forth tube at the first row. Only few of ash particles stick to the leeward side of the second tube at the first row. This may be due to the swing of the upstream flow. Combined with the results for stickiness and rebound efficiency, it can be known that, the rebound behaviour of impacting particles is dominant on the leeward side. The ash deposition mass on the leeward sides of the first, the second and the forth tubes at the second row is all from the stickiness of particles with a diameter of 11 μm. But for the third tube at different row, the deposition of large particles higher than 50 μm appears on its leeward side, due to periodic swing and vortex shedding of continuum phase flow.

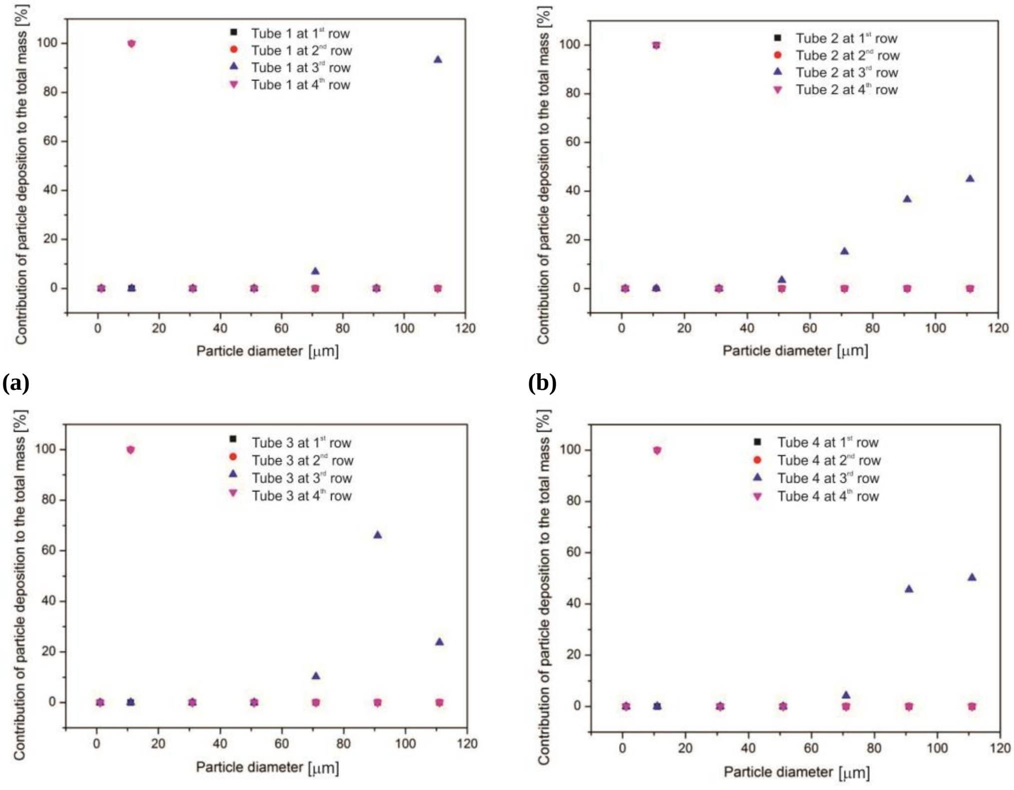

(a) **(b)**

(c) **(d)**

Figure 6. Contribution of deposition of ash particles to total deposition mass on the leeward side

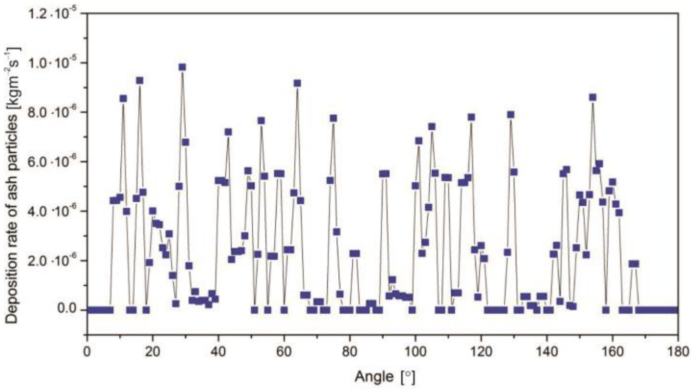

Figure 7. Deposition rate on the windward side of tube

Figure 7 presents the specific deposition rate around the node of windward side of the third tube at the first row. The *x* co-ordinate of 0° in fig. 7 is corresponding to the minimum value in Y-co-ordinate for the position of third tube at the first row in the computational domain. Similarly, the 180° is meant to the maximum value in Y-co-ordinate for the position of third tube at the first row in the computational domain. It can be found that the ash deposition is mainly centralized on the position with angle changed from 20° to 160°. But for other regions on the windward side of this tube, where the angle varies from 0° to 10° and from 170° to 180°, basically, there is no deposition occurred. This is because of less of ash particles involving into boundary-layer and then impacting on the surfaces within high flow velocity regions between tubes. Venturini *et al*. [3] found that the deposit is formed in a more narrow region where the angle changing from 50° to 130° due to the difference of injecting position in modelling simulation. Compared to the condensation rate of salt vapours on the windward side, the ash deposition rate has a same order of magnitudes. Due to less of ash deposition even no deposition appearing on the leeward side, the specific deposition rate is not given. Therefore, the condensation of salt vapours is dominant on the leeward side of tubes.

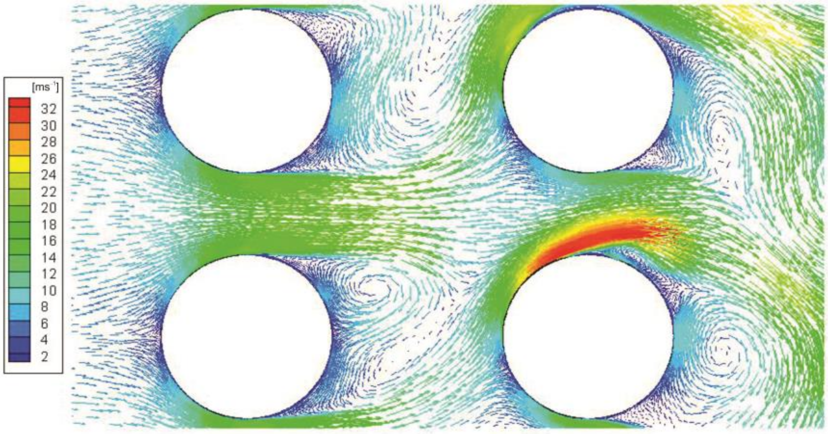

Figure 8. Instantaneous capture of velocity distribution at the local domain between two adjacent tubes

Figure 8 shows the flow velocity distribution between two adjacent tubes. After flowing over the first row, the flow becomes complex and more vortexes are generated. Meanwhile the number and the intensities of vortexes are increased. This condition easily forces some fine particles involving into the turbulent vortex, and then following motion with vortex at a long time until impacting and adhering on the surface or rebounding. Due to the periodic swing of flow, the stagnation position around the downstream tubes would also be changed.

Conclusions

In this work, 2-D computations on flue gas flow and biomass ash particles deposition were carried out, to obtain the sticking characteristic of ash particles and condensation rate of salt vapours on both of the windward and the leeward sides of tubes. Based on the predicted results, it can be known that the deposition rate of ash particles on the windward side is basically comparable with condensation rate of salt vapours. On the windward side of tubes at the first row, the sticking efficiency of impacting particles is high up to 70%, but no ash particles adhere on the leeward side. The sticking efficiency on the windward side of tube starts to increase after flowing over the second row, which can be higher than 50%. But on the leeward side of tubes, at the initial deposition stage the condensation effect of salt vapour is more important than ash particles stickiness. The ash deposition is appeared centrally on these positions of windward side with an angle changed from 20° to 160°. The condensation rate of $KCl_{(g)}$ is two orders of magnitude higher than that of $K_2SO_{4(g)}$ on both of the windward and the leeward side of tubes. The gas-to-solid conversion of salt vapors should be studied in future research.

Acknowledgment

The authors gratefully acknowledge financial support from the National Natural Science Foundation of China (No. 51906198 and 51876162).

References

[1] Yu, L. Y., *et al*., Study on Prediction Models of Biomass Ash Softening Temperature Based on Ash Composition, *J. Energy Inst.*, *87* (2014), 3, pp. 215-219
[2] Zhu, Y., *et al*., Modelling Study on the Effect of Ash Fusion Characteristics on the Biomass Slagging Behavior, *Thermal Science*, *22*(2018), 5, pp. 2113-2121
[3] Venturini, P., *et al*., Modelling of Particles Deposition in an Environment Relevant to Solid Fuel Boilers, *Appl. Therm. Eng.*, *49* (2012), Dec., pp. 131-138
[4] Garba, M. U., *et al*., Prediction of Potassium Chloride Sulphation and its Effect on Deposition in Biomass-Fired Boilers, *Energ. Fuel*, *26* (2012), 11, pp. 6501-6508
[5] Leppanen, A., *et al*., Numerical Modeling of Fine Particle and Deposit Formation in a Recovery Boiler, *Fuel*, *129* (2014), Aug., pp.45-53
[6] Weber, R., *et al*., On Predicting the Ash Behaviour Using Computational Fluid Dynamics, *Fuel Processing Technology*, *105* (2013), Jan., pp.113-128
[7] Mu, L., *et al*., Modelling and Measurements of the Characteristics of Ash Deposition and Distribution in a HRSG of Wastewater Incineration Plant, *Appl. Therm. Eng.*, *44* (2012), Nov., pp.57-68
[8] Perez, M. G., *et al*., 2-D Dynamic Mesh Model for Deposit Shape Prediction in Boiler Banks of Recovery Boilers with Different Tube Spacing Arrangements, *Fuel*, *158* (2015), Oct., pp.139-151
[9] Wang, Y., Tan, H., Condensation of KCl(g) Under Varied Temperature Gradient, *Fuel*, *237* (2019), Feb., pp.1141-1150
[10] Wang, Y., *et al*., The Condensation and Thermodynamic Characteristics of Alkali Compound Vapors on Wall During Wheat Straw Combustion, *Fuel*, *187* (2017), Jan., pp.33-42
[11] Akbar, S., *et al*., Modelling Potassium Release and the Effect of Potassium Chloride on Deposition Mechanisms for Coal and Biomass-Fired Boilers, *Combust. Theor. Model*, *14* (2010), 3, pp. 315-329
[12] Forstner, M., *et al*., CFD Simulation of Ash Deposit Formation in Fixed Bed Biomass Furnaces and Boilers, *Prog. Comput. Fluid Dy.*, *6* (2006), 4-5, pp. 248-261
[13] Niu, Y., *et al*., Slagging Characteristics on the Superheaters of a 12 MW Biomass-Fired Boiler, *Energy Fuels*, *24* (2010), 9, pp. 5222-5227
[14] Han, H., *et al*., A Parameter Study of Tube Bundle Heat Exchangers for Fouling Rate Reduction, *Int. J. Heat Mass Tran.*, *72* (2014), May, pp.210-221
[15] Haider, A., Levenspiel, O., Drag Coefficient and Terminal Velocity of Spherical and Nonspherical Particles, *Powder. Technol.*, *58* (1989), 1, pp. 63-70
[16] Tomeczek, J., *et al*., Two-Dimensional Modelling of Deposits Formation on Platen Superheaters in Pulverized Coal Boilers, *Fuel*, *88* (2009), 8, pp.1466-1471
[17] Kær, S. K., Extending the Capability of CFD Codes to Assess Ash Related Problems in Biomass Fired Boilers, *Proceedings*, 227th ACS Annual Meeting, Anaheim, Cal., USA, 2004,Vol. 47, pp.97-108
[18] Zhou, H., *et al*., Dynamic Mechanistic Model of Superheater Deposit Growth and Shedding in a Biomass Fired Grate Boiler, *Fuel*, *86* (2006), 10, pp.1519-1533

Paper submitted: March 11, 2020
Paper revised: April 25, 2020
Paper accepted: May 10, 2020